On neoclassical impurity transport in stellarator geometry

J. M. García-Regaña, R. Kleiber, C. D. Beidler, Y. Turkin, H. Maaßberg and P. Helander

Max-Planck-Institut für Plasmaphysik, EURATOM-Assoziation, Wendelsteinstr. 1, 17491 Greifswald, Germany

E-mail: jose.regana@ipp.mpg.de

Abstract. The impurity dynamics in stellarators has become an issue of moderate concern due to the inherent tendency of the impurities to accumulate in the core when the neoclassical ambipolar radial electric field points radially inwards (ion root regime). This accumulation can lead to collapse of the plasma due to radiative losses, and thus limit high performance plasma discharges in non-axisymmetric devices.
A quantitative description of the neoclassical impurity transport is complicated by the breakdown of the assumption of small $\mathbf{E}\times\mathbf{B}$ drift and trapping due to the electrostatic potential variation on a flux surface $\tilde{\Phi}$ compared to those due to the magnetic field gradient. The present work examines the impact of this potential variation on neoclassical impurity transport in the Large Helical Device (LHD) stellarator. It shows that the neoclassical impurity transport can be strongly affected by $\tilde{\Phi}$. The central numerical tool used is the δf particle in cell (PIC) Monte Carlo code `EUTERPE`. The $\tilde{\Phi}$ used in the calculations is provided by the neoclassical code `GSRAKE`. The possibility of obtaining a more general $\tilde{\Phi}$ self-consistently with `EUTERPE` is also addressed and a preliminary calculation is presented.

1. Introduction

Thermonuclear fusion would benefit from the achievement of quasi steady-state magnetic plasmas confinement with similar characteristics to those expected in a future reactor. In this respect the stellarator concept has an advantage over the pulsed tokamak. On the other hand the neoclassical transport exhibited by the former at low collisionality in the absence of electric fields, in the so-called $1/\nu$ regime, is considerably larger. The reason for this unfavourable behaviour is that in contrast to the axisymmetric case, where the collisionless trajectories of the trapped particle are confined, the orbits of particles trapped in the helical magnetic wells are generally not confined. This situation leads to a different radial transport rate for each species in the plasma and necessitates a radial electric field $\mathbf{E}_r = -\nabla\Phi_0$ that restores ambipolarity. Here $\Phi_0 = \Phi_0(s)$ is the lowest order electrostatic potential and only depends on the flux surface label. In the present work we use $s = \psi/\psi_0$, with ψ is the toroidal flux and ψ_0 the toroidal flux at the last closed magnetic surface. This label can be written in terms of the effective radius

r as $s \approx (r/a)^2$ with a the minor radius of the plasma. In the present context the basic ordering parameter, $\delta \equiv \rho/L$, is the Larmor radius ρ normalized to a typical macroscopic variation length scale L. Consequently the distribution function is expressible up to first order as $f \approx f_0 + \delta f$, with $\delta f/f_0 \sim O(\delta)$. In standard conditions $\mathbf{E}_r$ points inwards (ion root regime) and predicts accumulation of impurities [1]. The subsequent increase of radiative losses from the core can cause the collapse of the plasma [2, 3], and, in the worst case, endanger the capability of the stellarator to confine it in steady-state.

A quantitative and comprehensive description of the impurity dynamics requires not only the ambipolar radial electric field but also the electrostatic potential $\tilde{\Phi} = \Phi - \Phi_0$ determined by δf. This portion of the total electrostatic potential Φ, whose explicit solution has been obtained in the past [4, 5] and pointed out to have a modest impact on the transport of the bulk species [5, 6, 7] has been traditionally neglected. This rests on two assumptions. First, the radial $\mathbf{E} \times \mathbf{B}$ drift arising from $\tilde{\Phi}$,

$$\mathbf{v}_{\tilde{\Phi}} = -\frac{\nabla \tilde{\Phi} \times \mathbf{b}}{B}, \tag{1}$$

is assumed to be smaller than the curvature and *grad-B* drifts. In the vacuum approximation these are given by,

$$\mathbf{v}_{\mathrm{d}} = \frac{m}{q} \frac{\mu B + v_{\parallel}^2}{B^2} \mathbf{b} \times \nabla B, \tag{2}$$

with m the mass of the particle, $q = Ze$ its electric charge, Z is the charge number, e is the unit charge absolute value, B is the magnetic field strength, $\mathbf{b}$ is a unitary vector pointing in the direction of the magnetic field line, $\mu = v_{\perp}^2/2B$ is the magnetic moment, $v_{\parallel}$ is the parallel velocity and $v_{\perp}$ is the perpendicular one. It can be shown that the ratio between the absolute values of $\mathbf{v}_{\tilde{\Phi}}$ and $\mathbf{v}_{\mathrm{d}}$ is thus of order

$$\frac{v_{\tilde{\Phi}}}{v_{\mathrm{d}}} \sim \frac{Ze\tilde{\Phi}}{T} \frac{R}{a}, \tag{3}$$

where R is the major radius of the device, and it is assumed that the typical variation length scales for B and $\tilde{\Phi}$ are similar to R and a, respectively. This ratio can be acceptably small at low values of Z, but is usually considerable for heavy impurities.

Second, the parallel acceleration $a_{\parallel} = -(q/m)\mathbf{b} \cdot \nabla \tilde{\Phi}$ is assumed to be negligible compared to the mirror force $a_{\mathrm{m}} = -\mu \mathbf{b} \cdot \nabla B$. The ratio between these two is of order,

$$\frac{a_{\parallel}}{a_{\mathrm{m}}} \sim \frac{Ze\tilde{\Phi}}{T} \frac{B}{\Delta B}, \tag{4}$$

with ΔB the typical amplitude of the helical magnetic wells. Again, the proportionality to Z makes it necessary to account for $a_{\parallel}$ if the impurity transport is to be quantitatively obtained, although $\tilde{\Phi}$ can be sufficiently small for the bulk species.

On the other hand, the inclusion of $\tilde{\Phi}$ into the problem makes the kinetic energy of the impurities vary enough to violate the traditional neoclassical mono-energetic assumption

that the velocity is nearly constant along the collisionless particle orbits.
In the present work we put the focus on the computation of the neoclassical particle flux of impurities including $\tilde{\Phi}$, thus abandoning the mono-energetic assumption, but keeping the radially local one. This latter approximation assumes that the drifts across the flux surface are sufficiently small to treat them perturbatively. The calculations are performed with the Monte Carlo δf PIC code `EUTERPE`. A concise description of it is given in section 2, highlighting the truncation of the global characteristics to perform local neoclassical runs. Section 3 shows particle flux calculations for C^{6+}, Ne^{8+} and Fe^{20+} in the LHD standard configuration including the poloidal variation of $\tilde{\Phi}(\theta)$, with θ the poloidal coordinate. This is obtained from the solution of the steady-state ripple averaged drift kinetic equation obtained by the `GSRAKE` code [8]. Section 4 addresses the calculation of $\tilde{\Phi}$ by `EUTERPE`, discussing a preliminary result that includes the dependence of $\tilde{\Phi}$ on the toroidal coordinate ϕ and time t. Finally, in section 5 a summary of the results and a discussion are presented.

2. The `EUTERPE` code in the local neoclassical limit

`EUTERPE` is a global δf PIC Monte Carlo code, full-radius and full-flux surface, initially conceived for numerical simulation of linear gyro-kinetic micro-turbulence in 3D equilibria [9, 10, 11]. After undergoing successive updates the current version is non-linear, can treat multiple kinetic species simultaneously, and perform electro-magnetic simulations. Recently it has been extended to include pitch angle scattering collisions [12].
The set of phase space coordinates that `EUTERPE` uses is $\mathbf{z} = \{\mathbf{R}, v_\parallel, \mu\}$. $\mathbf{R}$ is the position of the guiding center of the particle in neoclassical runs, or its gyro-center in gyro-kinetic ones. In gyro-kinetic runs, the collisionless trajectory of a particle in phase space in the electrostatic limit, for simplicity written in the vacuum approximation ($\nabla \times \mathbf{B} \to 0$), is determined by the following set of equations:

$$\dot{\mathbf{R}} = \mathbf{v}_\parallel + \mathbf{v}_E + \mathbf{v}_\mathrm{d}, \tag{5}$$

$$\dot{v}_\parallel = \frac{q}{m}\mathbf{b}\cdot\mathbf{E} - \mu\mathbf{b}\cdot\nabla B + \frac{v_\parallel}{B^2}(\mathbf{b}\times\nabla B)\cdot\mathbf{E}, \tag{6}$$

$$\dot{\mu} = 0, \tag{7}$$

where a dot above a symbol denotes a time derivative, $\mathbf{E} = -\nabla\Phi$ is the electric field, $\mathbf{v}_E = \mathbf{E}\times\mathbf{b}/B$ and Φ the electrostatic potential obtained from the gyro-kinetic quasi-neutrality equation with arbitrary spatial dependence. The departure of the distribution function from the lowest order part f_0, $\delta f(\mathbf{z}, t)$, is simulated using markers, whose trajectories are pushed according to eqs. (5)-(7),periodically interrupted by the application of a random change of their pitch angle to account for collisions [13].
It is straightforward to prove that eqs. (5)-(7) conserve the total energy of the particle and preserve the incompressibility of the phase space flow, i.e. $\dot{\mathcal{E}} = 0$ with $\mathcal{E} =$

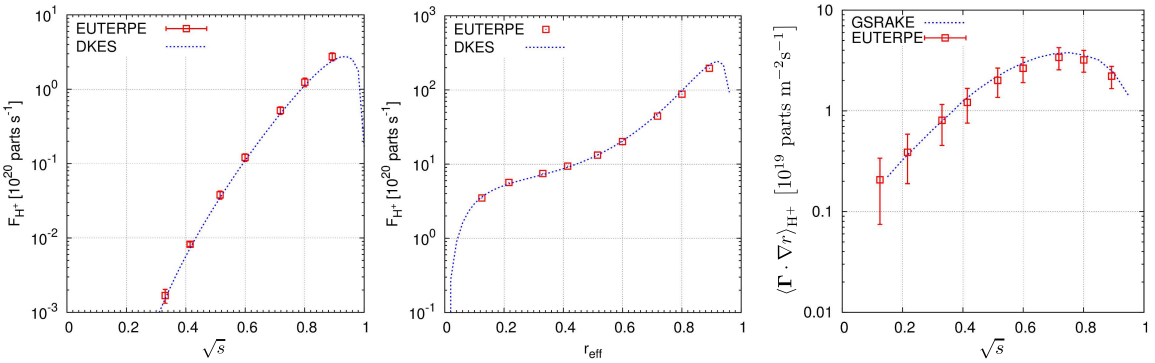

Figure 1: Particle flux of hydrogen in an axisymmetric circular cross section tokamak for the radial density flat profile of $n = 10^{20}$ m^{-3} and a temperature profile $T = 2(1-s)$ keV (left), and for $n = (1-s^4)\times 10^{19}$ m^{-3} at a fixed temperature of $T = 2$ keV (center). In the right, particle flux density of hydrogen in LHD for the profiles $n = (6-5s^4)\times 10^{19}$ m^{-3} and $T = (2-1.8s)$ keV including E_r.

$v_\parallel^2/2 + \mu B + (q/m)\Phi$ and $\nabla_{\mathbf{z}} \cdot (\mathcal{J}\dot{\mathbf{z}}) = 0$ with $\nabla_{\mathbf{z}} = \left(\nabla, \partial_{v_\parallel}, \partial_\mu\right)$ and $\mathcal{J} = B$ the Jacobian of our transformation.

The trajectory in real space followed by a particle given by eq. (5) is referred to as *global* since the radial magnetic and $\mathbf{E}\times\mathbf{B}$ drifts across the flux surface, $\mathbf{v}_{\mathrm{d}} \cdot \nabla s$ and $\mathbf{v}_E \cdot \nabla s$ respectively, are accounted for. In contrast, the guiding center trajectory without these drifts in lowest order is called *local*. Local trajectories find routine application in neoclassical simulations and follow from assuming $\Phi \approx \Phi_0$, resulting in $\mathbf{v}_E$ laying on the flux surface, and $v_{\mathrm{d}}/v_\parallel \sim \delta$. This avoids the introduction of a radial derivative in $\partial\delta f/\partial s$ into the kinetic equation, which increases the dimensionality of the problem. In this approximation the total energy is not conserved since the neglect of $\mathbf{v}_{\mathrm{d}}$ unbalances a cancellation in $\dot{\mathcal{E}}$ resulting in $\dot{\mathcal{E}} = -(q/m)\mathbf{v}_{\mathrm{d}} \cdot \nabla\Phi_0$. For impurities we need to retain $\tilde{\Phi}$ though, and assume that $v_{\tilde{\Phi}}/v_\parallel \sim \delta$ to preserve the local *ansatz*. This and the approximation $\mathbf{b}\times\nabla B\cdot\nabla\Phi \approx \mathbf{b}\times\nabla B\cdot\nabla\Phi_0$ brings additional non-conservation (of comparable magnitude) associated with $\tilde{\Phi}$: $\dot{\mathcal{E}} = -(q/m)\mathbf{v}_{\mathrm{d}} \cdot \nabla\Phi_0 - (q/m)\mathbf{v}_{\tilde{\Phi}} \cdot \nabla\Phi_0$ and $\dot{\mathcal{E}}_0 = -(q/m)\mathbf{v}_{\mathrm{d}} \cdot \nabla\Phi_0 - (q/m)v_\parallel \mathbf{b} \cdot \nabla\tilde{\Phi}$ where $\mathcal{E}_0 = v_\parallel^2/2 + \mu B + (q/m)\Phi_0$. The variation of the energy during one collisional time τ can be estimated as $(\Delta\mathcal{E})_\tau/T \lesssim (q\Phi_0/T)/(\Delta r/a)$, with $\Delta r \lesssim \delta v_\parallel \tau$ the scale of the total radial drift in a typical collisional time, and $\nabla \sim a^{-1}$.

Our equations for the marker trajectory in phase space for a local neoclassical run are thus,

$$\dot{\mathbf{R}} = \mathbf{v}_\parallel + \mathbf{v}_{E0}, \tag{8}$$

$$\dot{v}_\parallel = -\frac{q}{m}\mathbf{b}\cdot\nabla\tilde{\Phi} - \mu\mathbf{b}\cdot\nabla B + \frac{v_\parallel}{B^2}(\mathbf{b}\times\nabla B)\cdot\mathbf{E}_r, \tag{9}$$

$$\dot{\mu} = 0, \tag{10}$$

with $\mathbf{v}_{E0} = \mathbf{E}_r \times \mathbf{b}/B$. For the tokamak, where the small-$\mathbf{E}_r$ limit $v_{E0}/v_\parallel \sim \delta$ applies [14] (unless the plasma rotates rapidly) the second term in eq. (8) and the third in eq. (9) are neglected. Assuming that f_0 is a Maxwellian distribution function $f_0 = f_\mathrm{M}(s, v_\parallel, v_\perp) = \left[n_0(s)/(2\pi)^{3/2} v_\mathrm{th}^3(s)\right] \exp\left[-\left(v_\parallel^2 + v_\perp^2\right)/2v_\mathrm{th}^2(s)\right]$, with $v_\mathrm{th} = \sqrt{T/m}$ and $T = T(s)$ the temperature, the resulting kinetic equation reads as follows:

$$\begin{aligned}\frac{\partial \delta f}{\partial t} + \dot{\mathbf{R}} \cdot \nabla \delta f + \dot{v}_\parallel \frac{\partial \delta f}{\partial v_\parallel} = &- f_\mathrm{M} \left[\frac{1}{n}\frac{\partial n}{\partial s} + \left(\frac{mv^2}{2T} - \frac{3}{2}\right)\frac{1}{T}\frac{\partial T}{\partial s}\right](\mathbf{v}_\mathrm{d} + \mathbf{v}_{\tilde{\Phi}}) \cdot \nabla s + \\ &+ \frac{q}{m}\frac{f_\mathrm{M}}{v_\mathrm{th}^2}\left(\mathbf{v}_\parallel + \mathbf{v}_\mathrm{d}\right) \cdot \left(\mathbf{E}_r - \nabla\tilde{\Phi}\right).\end{aligned} \tag{11}$$

Note that in obtaining eq. (11) the original drift, eq. (5), was considered and those terms higher than first order in δ were truncated. Moreover since the approximation $\tilde{\Phi} \ll \Phi_0$ still holds the radial electric field related to $\tilde{\Phi}$ is considered negligible compared to $\mathbf{E}_r$. `EUTERPE`, in the present neoclassical modality, was satisfactorily benchmarked against theory and the codes `DKES` and `GSRAKE`. Figure 1 shows a comparison between the particle fluxes obtained with these codes in different cases. It is important to remark that in this comparison $\tilde{\Phi}$ is missing since `DKES` and `GSRAKE` assume mono-energetic trajectories.

3. Impurity particle transport in the presence of $\tilde{\Phi}(\theta)$

The code `GSRAKE` solves the ripple-averaged drift kinetic equation providing, apart from the neoclassical fluxes, the first order corrections to the equilibrium density and electrostatic potential $\tilde{n}(r, \theta)$ and $\tilde{\Phi}(r, \theta)$. The magnetic configuration is accounted for by means of a multiple-helicity model and the bounce average is performed along the toroidal coordinate ϕ. Moments of the perturbed distribution function and the flux-surface-average are defined in the *reduced* phase-space, in which the toroidal angle coordinate has been eliminated by performing the ripple average. This process *removes* the ϕ dependence of B appearing in the Jacobian of the initial phase-space. The resulting θ-dependent $\tilde{n}$ and $\tilde{\Phi}$ are written in Fourier series, and their coefficients are iteratively adjusted to simultaneously fulfill the quasi-neutrality and ambipolarity constraints among bulk ions and electrons (for the details of the code see refs. [8, 7]).

In the present section the E_r and $\tilde{\Phi}$ obtained with `GSRAKE` for two different sets of density and temperature profiles have been used as input for `EUTERPE`, which in turn obtains the particle flux density $\langle \mathbf{\Gamma} \cdot \nabla r \rangle$. This particular choice of tasks is due to the fact that `EUTERPE` is capable to integrate the impurity trajectories in the 4D phase space resulting from the breakdown of the mono-energetic approximation for impurities while `GSRAKE` is not. On the other hand, due to the radial locality of the trajectories E_r cannot be computed by `EUTERPE` unless that this is performed iteratively, which adds an unnecessary computational cost due the slow convergence of the fluxes for the bulk species. The

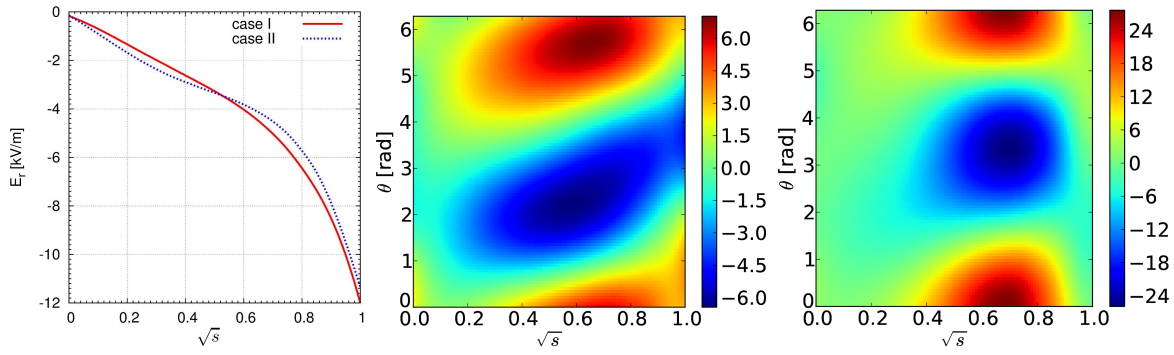

(a) (b) (c)

Figure 2: (a) Ambipolar radial electric field obtained with GSRAKE in the two cases considered for the impurity runs launched by EUTERPE. The corresponding $\tilde{\Phi}$ are represented in plot (b) for case I, and (c) for case II.

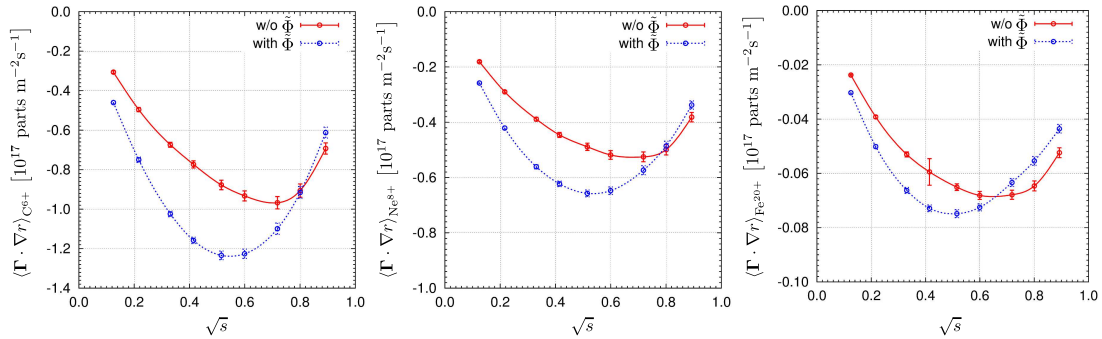

(a) (b) (c)

Figure 3: Particle flux density of C^{6+} (a), Ne^{8+} (b) and Fe^{20+} (c) as a function of $\sqrt{s}$ in LHD for the set of profiles considered in case I (see text).

magnetic equilibrium considered corresponds to the standard LHD configuration with $R \approx 3.73$ m, $a \approx 0.6$ m and $B_{00}(\sqrt{s} = 0.5) = 2.53$ T. Two cases have been considered and are labeled as *case I* and *case II*. The equilibrium temperature and density profiles considered in the former case for the bulk ions (hydrogen) are $n = (6 - 5s^4) \times 10^{19}$ m^{-3} and $T = (2 - 1.8s)$ keV. The rather lower collisional case II considers instead $n = 5(1 - 0.2s^4) \times 10^{19}$ and $T = 3(1 - 0.93s)$. The temperature profiles are taken to be the same for electrons and impurities, and their central density are adjusted to fulfill quasi-neutrality. The effective charge is set to $Z_{\text{eff}} = 1.05$ at all radii. In fig. 2(a) the ambipolar radial electric field is displayed for both pairs of profiles, in fig. 2(b) the $\tilde{\Phi}$ map dependent on $\sqrt{s}$ and θ for case I is given, while 2(c) represents the one corresponding to the case II.

The simulations run with EUTERPE were carried out for C^{6+}, Ne^{8+} and Fe^{20+}. The radial profiles of the particle flux density are shown in figs. 3(a)-(c) for case I. In this set of

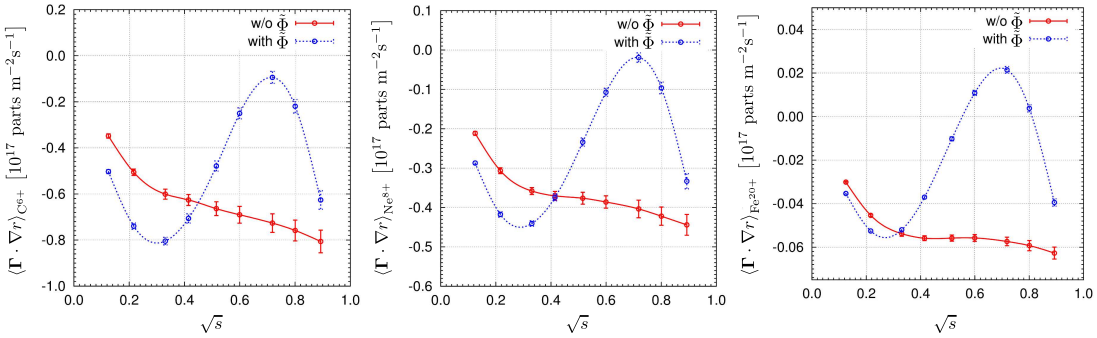

(a) (b) (c)

Figure 4: Particle flux density of C^{6+} (a), Ne^{8+} (b) and Fe^{20+} (c) as a function of $\sqrt{s}$ in LHD for the set of profiles considered in case II (see text).

plots the impact of $\tilde{\Phi}$ on the three species is detrimental up to $\sqrt{s} \approx 0.7 - 0.8$ from the impurity accumulation perspective. From that radial location outwards the trend is reversed and the inward flux in the presence of $\tilde{\Phi}$ becomes weaker. We conclude that $\tilde{\Phi}$ can act either to amplify or mitigate the inward flux driven by $\mathbf{E}_r$. It can also be observed that $\tilde{\Phi}$ affects the C^{6+} particle flux more than Fe^{20+}'s. At a first glance this may look like contradictory with what eqs. (3) and (4) suggest. But it is important to notice that what those expressions imply is that the acceleration due to $\tilde{\Phi}$ must be included in $\dot{v}_{\|}$ and that $\mathbf{v}_{\tilde{\Phi}}$ must be put on the same order than $\mathbf{v}_{\rm d}$. This in turn brings to the source of the kinetic equation, eq. (11), three more terms traditionally neglected containing $\tilde{\Phi}$. The balance of these terms with the rest and with each other does not necessarily lead to a more noticeable impact on the transport produced by $\tilde{\Phi}$ with the increasing Z.

The same behavior is shown for case II in figs. 4(a)-(c). Again $\tilde{\Phi}$ breaks the monotonic growth of the inward impurity flux with increasing s. The change in the trend is observed at a different radial location than in case I, $\sqrt{s} \approx 0.3 - 0.4$, which corresponds to almost the position where the electrostatic potential starts to be appreciably large, see figure 2(c). A remarkable feature in this case is that the particle flux approaches the value of zero at $\sqrt{s} \approx 0.7$ for C^{6+} and Ne^{8+} and is even positive for Fe^{20+}. That radial position corresponds to the maximum amplitude of $\tilde{\Phi}$ along θ.

At this point it is convenient to recall the discussion about the weight of $\tilde{\Phi}$ for driving radial transport and trapping particles reflected by the expressions (3) and (4). First, it is important to notice that in case I the variation of $\tilde{\Phi}$ leads to an electrostatic energy variation of approximately 1% of the thermal energy for a unit charge. In case II the same variation would result in approximately a 2% change. This indicates that the strong change in the behavior of the particle flux cannot be explained by such increase in the ratio $q\tilde{\Phi}/T$ exclusively. This points out also to the non-trivial interplay between all terms in the kinetic equation with and without $\tilde{\Phi}$. This may lead to the natural question of how much the transport of hydrogen nuclei can be affected by $\tilde{\Phi}$. In figure

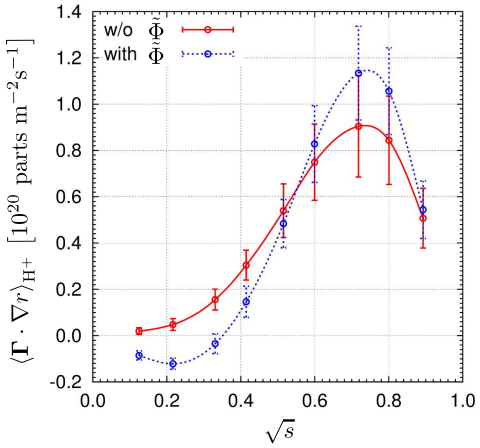

Figure 5: Particle flux density of H^+ as a function of $\sqrt{s}$ in LHD for the case II profiles (see text).

(5) the comparison between the particle flux density of H^+ with and without $\tilde{\Phi}$ for the case II is represented. The profiles does not change qualitatively as in the case of impurities. Nevertheless two important features should be emphasized. On the one hand the flux turns to be negative below $\sqrt{s} < 0.3$ under the action of $\tilde{\Phi}$, and on the other the value at its maximum is enhanced in an approximately a 20 %. These changes, although not as significant as in the cases with impurities, represent a noticeable effect.

4. The self-consistent calculation of $\tilde{\Phi}(\theta, \phi, t)$ in EUTERPE

In light of these results it is of immediate interest to extend the calculations to account for the toroidal dependence of $\tilde{\Phi}$. Apart from the role that this can play, it is important to remember that the ripple average also reduces the number of possible configurations that can be studied. Although this is beyond the scope of the present work, we show in this section a preliminary result where $\tilde{\Phi}(\theta, \phi, t)$ is obtained self-consistently with EUTERPE. The approach rests on the fulfilment of the neutrality condition on the density perturbations for each species, $\sum_s \tilde{n}_s = 0$. The starting point is the quasi-neutrality gyro-kinetic equation [15] that the code solves at each time step. Considering for simplicity kinetic ions and adiabatic electrons, the equation reads as follows:

$$e \langle \tilde{n}_i \rangle + m_i \nabla \cdot \left(\frac{n_{0i}}{B^2} \nabla_\perp \tilde{\Phi} \right) - \frac{e^2 n_{0e}}{T_e} \left(\tilde{\Phi} - \bar{\Phi} \right) = 0, \tag{12}$$

where the lower indices i and e denote bulk ions and electrons respectively, n_0 is the equilibrium density, $\langle \tilde{n}_i \rangle$ is the gyro-averaged ion density, $\bar{\Phi}$ is the flux-surface averaged electrostatic potential, and m_i the ion mass. The equation is simplified by invoking the limit $k_\perp \rho \ll 1$ with $k_\perp$ the perpendicular characteristic wave-length of the fluctuations. Since the second term in eq. (12) is a factor $k_\perp^2 \rho^2$ smaller than the others it can be neglected. In addition, the gyro-average operation is unnecessary in drift kinetics. And

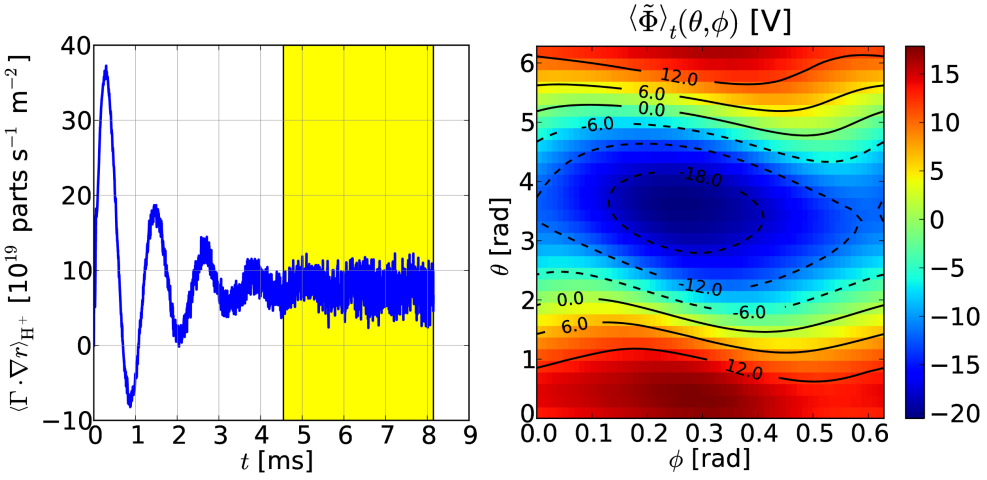

(a) (b)

Figure 6: (a) Time dependent flux of hydrogen in LHD for the case II profiles (see text in section 3) at $\sqrt{s} = 0.5$. (b) Time averaged electrostatic potential $\langle \tilde{\Phi} \rangle_t(\theta, \phi)$.

finally, by flux surface averaging of the remaining expression, it can be shown that $\bar{\Phi} = \tilde{\Phi}_{0,0} = 0$. The sub-indices in $\tilde{\Phi}$ denote that the poloidal and toroidal mode numbers, m and n respectively, are both equal to zero. The final expression is then:

$$\tilde{n}_i = \frac{e}{T_e} n_{0e} \tilde{\Phi}. \tag{13}$$

In order to prevent the code from developing short wave-length unstable modes, only low mode numbers are retained by employing a spectral filter set to $0 \leq m \leq 4$ and $-4 \leq n \leq 4$. Since the trajectories are radially local, it is difficult to calculate E_r. An iterative adjustment of E_r until ambipolarity is fulfilled is not feasible due to the dynamic nature of the simulation, which makes it impossible to determine the flux before it has saturated. Thus, E_r is imposed externally.

Figures 6(a)-(b) show the result of a simulation for $\tilde{\Phi}(\theta, \phi, t)$ at $\sqrt{s} = 0.5$, considering the profiles of the labeled as case II in section 3. The calculation of both the hydrogen flux density $\langle \mathbf{\Gamma} \cdot \nabla r \rangle_{H^+}$ and $\tilde{\Phi}$ is dynamical, as has already been mentioned. In figure 6(a) $\langle \mathbf{\Gamma} \cdot \nabla r \rangle_{H^+}$ is shown as a function of time. Once it has reached the stationary value, a time average of the potential is performed. The resulting time averaged potential $\langle \tilde{\Phi} \rangle_t(\theta, \phi)$ is represented in fig. 6(b). The time interval considered for the average is colored yellow in fig. 6(a). It can be noticed that a weak but appreciable variation of $\tilde{\Phi}$ with ϕ is present.

5. Summary and discussion

In the present work we have considered the problem of impurity particle transport in stellarator geometry. Impurity accumulation can occur under certain plasma conditions

and is predicted by the standard local and mono-energetic neoclassical theory.
Nevertheless, the mono-energetic approximation may not hold for impurities, whose high charge makes them sensitive to electrostatic potential variations within the flux surface. This makes the problem at least – assuming radial locality of the trajectories in the lowest order – a 4D problem. The task of solving it to obtain the impurity particle flux density has been considered by the Monte-Carlo code `EUTERPE`. The potential $\tilde{\Phi}(\theta)$ arising by enforcing quasi-neutrality in the code `GSRAKE` was used as input for the `EUTERPE` runs.
The results have shown that $\tilde{\Phi}$ can both increase and decrease the impurity accumulation, depending on the interplay between the radial drives $\mathbf{v}_{\tilde{\Phi}}$ and $\mathbf{v}_{\mathrm{d}}$ and the electrostatic and magnetic trapping. These, in turn, have shown to be determined ultimately by the spectrum of $\tilde{\Phi}$ rather than by its absolute value. The calculations show that the inward flux of impurities can be suppressed completely.
Future work aims at a self-consistent calculation of $\tilde{\Phi}$ by `EUTERPE` along the line that has been presented. The preparation of a global neoclassical version of the code, which would allow E_r to be computed, is also forthcoming.

6. Acknowledgements

This work was supported by EURATOM and carried out within the framework of the European Fusion Development Agreement. The views and opinions expressed herein do not necessarily reflect those of the European Commision.
Part of the calculations were carried out using the HELIOS supercomputer system at Computational Simulation Centre of International Fusion Energy Research Centre (IFERC-CSC), Aomori, Japan, under the Broader Approach collaboration between Euratom and Japan, implemented by Fusion for Energy and JAEA. This work was also granted access to the HPC resources of HPC-FF made available within the Distributed European Computing Initiative by the PRACE-2IP, receiving funding from the European Community's Seventh Framework Programme (FP7/2007-2013) under grant agreement no. RI-283493.
J M García-Regaña wishes to thank K. Kauffmann for her helpful comments and the second referee for the constructive suggestions.

References

[1] H Maaßberg *et al* 1999 *Plasma Phys. and Control. Fusion* **41** 1135.
[2] M Hirsch *et al* 2008 *Plasma Phys. and Control. Fusion* **50** 053001.
[3] Y Nakamura *et al* 2002 *Plasma Phys. and Control. Fusion* **44** 2121.
[4] D R Dobrott and J L Johnson 1969 *Plasma Phys.* **11** 211.
[5] H Mynick 1984 *Phys. Fluids* **27**(8) 2086.
[6] D D -M Ho and R M Kulsrud 1987 *Phys. Fluids* **30**(2) 442.
[7] C D Beidler and H Maaßberg 2005 *15th International Stellarator Workshop, Madrid*.
[8] C D Beidler and W D D'haeseleer 1995 *Plasma Phys. and Control. Fusion* **37** 463.
[9] G Jost *et al* 2001 *Phys. Plasmas* **8** 3321.

[10] V Kornilov *et al* 2005 *Nucl. Fusion* **45**(4) 238.
[11] R Kleiber 2006 *AIP Conference Proceedings* **871** 136.
[12] K Kauffmann *et al* 2010 *J. Phys.: Conf. Ser.* **260** (1) 012014.
[13] T Takizuka 1977 *J. Comp. Phys.* **25** (3) 205.
[14] P Helander and D J Sigmar 2001 *Collisional transport in magnetized plasmas*, Cambridge University Press.
[15] T S Hahm 1988 *Phys. Fluids* **31** (9) 2670.